Numerical simulation for diffusion process by the Kelvin-Helmholtz instability

Akiko Mano　Tetuya Kawamura

(Received May 23, 2011)

Abstract

The Kelvin-Helmholtz instability is numerically simulated to investigate the diffusion process of fine sediment maintaining on the sea surface. A realistic sediment distribution at the Rhone River estuaries is shown and the numerical simulation is carried out under the realistic wind condition. The following features are found out: (1)the initial strong impact caused by the gust wind on the sea surface can induce the Kelvin-Helmholtz instability, and induce the vertical mixing. (2)the mean wind speed, temperature differences and salinity differences do not play significant roles for inducing the Kelvin-Helmholtz instability.

1 INTRODUCTION

The Rhone River is located in the south of France, a part of Gulf of Lions. The gulf has a large continental shelf, and is paid large attention to the sediment fate on it to understand the ecosystem. The diffusion process of sediment maintaining on the sea surface layer is considered in this study. There are occasions when the fine sediment spreads over the sea surface for several days, such as from June 18 to 25 in 2008. Several studies mentioned that the strong buoyant force traps fine sediment on the surface layer. There are some pycnoclines in water column in the sea, and the difference of density may prevent the light upper layer and the heavy lower layer the layers from mixing each other. In such cases, the light upper layer is maintained for a while with fine sediment floating in its layer. The one of factors inducing vertical mixing across the boundary of the layers is considered as the Kelvin-Helmholtz instability(Kashiwamura, 1978). Our objective is to investigate the influence of Kelvin-Helmholtz instability on the boundary of the pycnocline. The difference of salinity, temperature and wind condition are considered. The diffusion process is also described.

2 Computational Method

The governing equations are the incompressible Navier-Stokes equations with Boussinesq approximation. The governing equations are as follows(Komurasaki, 2007):

$$\mathrm{div}\,\mathbf{u} = 0 \tag{1}$$

$$\frac{D\mathbf{u}}{Dt} = -\frac{1}{\rho}\mathbf{grad}\ \delta p + \frac{1}{\rho}\mu\triangle\mathbf{u} + \mathbf{F} \tag{2}$$

$$\mathbf{F} = (\ 0,\ 0,\ \frac{\rho_w}{\rho}(\beta(T-T_b) - (S-S_b))g\ ) \tag{3}$$

$$\frac{DT}{Dt} = \frac{1}{\rho}\kappa_T\triangle T \tag{4}$$

$$\frac{DS}{Dt} = \frac{1}{\rho}\kappa_S\triangle S \tag{5}$$

$$\rho = \rho_w + \rho_w S \tag{6}$$

$$\delta p = p - p_b \tag{7}$$

where $\mathbf{u}$ is velocity, t is time, ρ is density, μ is viscosity, u and v are velocity components in x and y axis directions, ρ_w is density of water at reference temperature, β is coefficient of volume expansion, T is temperature, T_b is base temperature, S is salinity, S_b is base salinity, g is gravity acceleration. κ_T is thermal diffusion coefficient, κ_S is salinity diffusion coefficient, p is pressure, and p_b is base pressure.

They can be solved by the fractional step method.

2.1 Discretization

Computational domain is a rectangular solid that is divided by the grid of 100 × 10 × 60. The Cartesian coordinate system is used. The two layer structure is considered, upper layer is regarded as

the brackish water, and lower layer is regarded as sea water. The axes of x, y, and z correspond to wind direction or applied initial velocity direction, traverse direction, and vertical upward direction, respectively. The second-order accurate central-difference scheme and the Euler explicit method are used.

2.2 Initial condition

The reference speed is virtually 1 m/s. The reference length is 40×10^{-6} m. The reference time is 40×10^{-6} second. The reference temperature(T_{ref}) has a range of -1 to 5. The reference difference salinity(S_{ref}) has a range of 0.0001 to 0.004.
Each value at the upper layer is initially set as follows:

$$\mathbf{u} = (u_{ini},\ 0,\ 0) \tag{8}$$

$$T = S = 0 \tag{9}$$

Each value at the lower layer is initially set as follows:

$$\mathbf{u} = (0,\ 0,\ 0) \tag{10}$$

$$T = S = 1 \tag{11}$$

2.3 Boundary condition

At the bottom boundary:

$$\mathbf{u} = (u_{wind},\ 0,\ 0) \tag{12}$$

$$T = S = 1 \tag{13}$$

$$p = g\int \rho\, dz \tag{14}$$

At the surface boundary:

$$\mathbf{u} = (u_{wind},\ 0,\ 0) \tag{15}$$

$$T = S = p = 0 \tag{16}$$

where u_{wind} is determined from the wind condition.
Periodic boundary conditions are applied to both y and z directions.

2.4 Parameters

Cases 1 to 16 shown in Table 1 are studied. Wind force affects sea surface in 3.5 % (Madsen, 1997). Thus the following value is used.

$$u_{wind} = U_{wind}\frac{3.5}{100} \tag{17}$$

where U_{wind} is wind speed that depends on each case(see Table 1).

$\rho_w = 1000, \mu = 854.4\times10^{-6}, g = 9.8, \beta = 0.21\times10^{-3}, \kappa_T = 1.453\times10^{-4}, \kappa_S = 1.453\times10^{-6}$, in meter-kilogram-second system. These values are based on the study of Komurasaki(2007).
$T_b = 285.5, S_b = 0.034$. Both correspond to the situation at the surface brackish layer(Estournel, 2001).
In the Estournel's study, the salinity of sea water is 0.038. The computations using the reference difference salinity of 0.004 correspond to the difference between the brackish layer and the sea water. Nevertheless, the brackish layer thickness is about 2 m. To investigate the influence of the computational layer(depth) thickness that is quite small, the computation using the reference temperature/salinity differences of 0.01/0.0001 are also carried out.
Time increment δt is set enough small to compute.

Table 1: Parameters of each computation.

Case	u_{ini}[m/s]	U_{wind}[m/s]	T_{ref}[°C]	S_{ref}
1	1	0	1	0.004
2	1	7	1	0.004
3	1	20	1	0.004
4	2	0	1	0.004
5	3	0	1	0.004
6	4	0	1	0.004
7	0.35	5	1	0.004
8	0.49	5	1	0.004
9	1.4	5	1	0.004
10	3	5	1	0.004
11	5	5	1	0.004
12	7	5	1	0.004
13	0.49	5	0.01	0.004
14	3	5	-1	0.004
15	3	5	5	0.004
16	0.49	5	1	0.0001

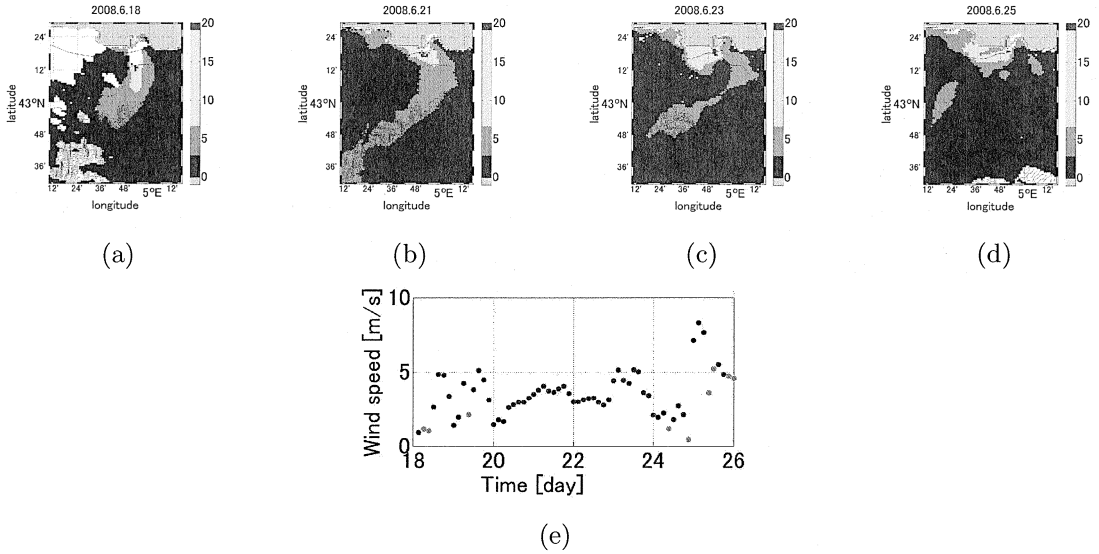

Fig.1: Satellite images and wind force. (The white area is missing data due to the cloud.)

3 Observation data

To obtain the observed distribution of sediment at the sea surface, SPM(suspended particle matters) distribution from the satellite images derived from MODIS are used. The SPM distribution can be used as a tracer of the plume. Two images are taken into account. The date are obtained on June 18, 21, 23 and 25 in 2008 as shown in the images of Fig.1. For simplify, the concentration of SPM is classified into 4 ranges: under 3 mg/l, 3 to 7 mg/l, 7 to 20 mg/l, over 20 mg/l as shown with the color bar. To see the plume extent, the plume represented by the concentration of 3 mg/l is considered as the proper threshold. Although each particle of sediment has its settling velocity depending on its density and its diameter, the small concentration area for SPM is regarded as being kept in the plume area for a while because the density and diameter are low and small enough to float in brackish layer at the sea surface, and play a role as the plume tracer.

Fig.1 shows a phenomenon given by SPM distribution of the Rhone River plume from June 18 to June 25 with the wind speed. This wind speed is provided MM5 meteorological models at 10m above the sea surface off the Rhone river mouth. The term from June 18 to 23 is the term under the remarkable weak continuous southern wind condition with the speed of 3 to 5 m/s. The SPM distribution remains for this term without diffusion. In this situation, it is considered that the upper layer that is brackish water and the lower layer that is salt water keep the two layer structure without mixing.

On June 25, the remaining SPM distribution seems to disappear. Nevertheless, the SPM distribution at the left-middle part of the Fig.1(d) is remained from June 23. The wind speed is about 7 m/s during the term. This implies that the strong wind may induce diffusion of SPM distribution at the sea surface.

4 Computational Results and discussion

4.1 impact of wind speed

Fig.2 shows the computational results from Case 1 to 3. This series is investigated in order to see the impact of wind speed on the two layer boundary. The initial velocity at the upper layer is fixed to 1, and each wind condition is applied(See Table 1). The shading represents the density field. The range is from 1034 to 1038, that corresponds to the initial density for the upper layer and the lower layer. This range is used hereafter through this paper.

Fig.2(a) shows the condition of no wind. The instability between the upper layer and the lower layer is not induced and the boundary of the two layers remains clearly. The mixing and diffusion processes

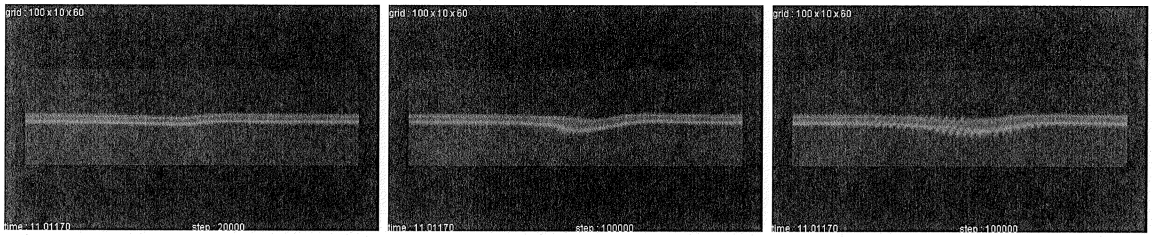

(a) $U_{wind} = 0$. (Case 1) (b) $U_{wind} = 7$. (Case 2) (c) $U_{wind} = 20$. (Case 4)

Fig.2: Computational results for impact of wind speed. $U_{ini} = 1$ for each case. The shading represents density field. The same range of density is used for each case.

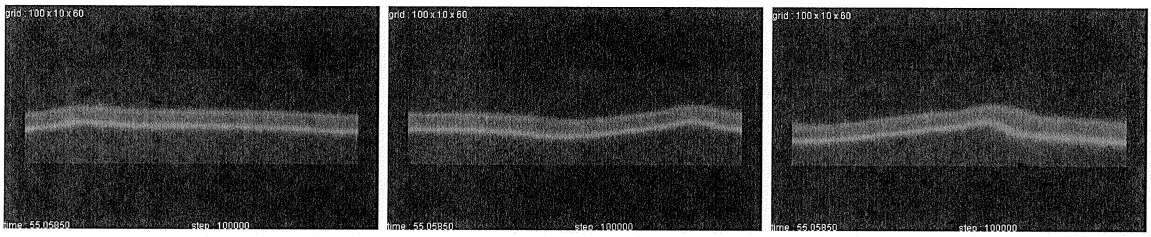

(a) $U_{ini} = 2$. (b) $U_{ini} = 3$. (c) $U_{ini} = 4$.

Fig.3: Computational results for impact of initial velocity under no wind condition. The shading represents density field. The same range of density is used for each case.

are not induced in this case.

According to Fig.2(a), (b) and (c), the instability becomes larger as the wind speed increases. Nevertheless, the Kelvin-Helmholtz instability that can induce the vertical mixing is too small to mix the two layers. Thus these figures suggest that the wind force is not an important factor for vertical mixing.

4.2 impact of initial velocity

Fig.3 shows the computational results for Case 4 to 6. This series is investigated in order to see the impact of the initial velocity on the two layer boundary. The wind speed is fixed to 0 m/s, and each initial velocity is applied.

Fig.3(a), (b) and (c) show the situation that the initial velocity at the upper layer is 2, 3 and 4. Although the boundary of the two layers remains clearly, it is obvious that the instability increases as the initial velocity increases compared with the series shown in Fig.2. Thus these figures suggest that the initial velocity has more impact on the instability than the wind speed.

4.3 realistic velocity field application

Fig.4 shows the computational results for Case 7 to 12. The series from Case 7 to 9 is investigated in order to see correspondence with the actual wind condition. The initial velocity is regarded as the instantaneous strong gust wind. The situation is taken into account when the wind blows with the speed of 5 m/s continuously and the gust wind blows with various speed at the first step. Thus the wind speed is fixed to 5 m/s, and each initial velocity is applied so that it corresponds to actual wind speed. As the wind speed goes generally up to 20 m/s in this region, the gust wind can be regarded to reach the speed of 40 m/s because the gust wind can blow 1.5 to 2 times or more as much as the mean wind speed. The expected wind speed and the corresponding initial velocity are shown in Table 2 as the reference.

In this series, the boundary between the two layers is keeping in Fig.4(a) and (b), however, the first symptom of breaking can be seen in Fig.4(c). This is due to Kelvin-Helmholtz instability. Thus it is proved that the Kelvin-Helmholtz instability can break the boundary by actual wind force.

In addition, the initial velocity in Fig.4(a) and (b)

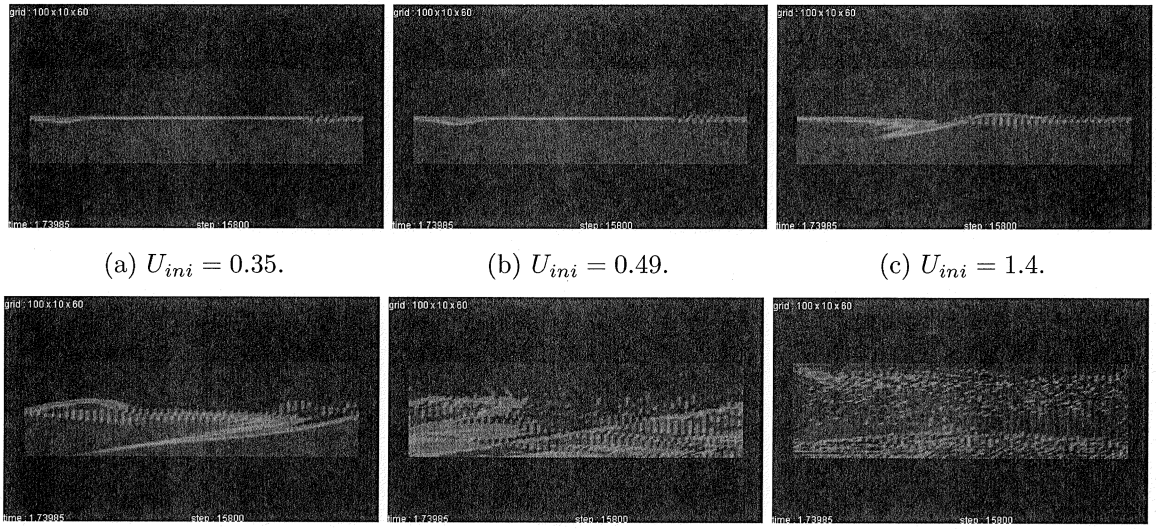

(a) $U_{ini} = 0.35$. (b) $U_{ini} = 0.49$. (c) $U_{ini} = 1.4$.

(d) $U_{ini} = 3$. (e) $U_{ini} = 5$. (f) $U_{ini} = 7$.

Fig.4: Computational results for impact of initial velocity with wind speed of 5 m/s. The shading represents density field. The same range of density is used for each case.

corresponds to the gust wind speed when the wind blows with 5 m/s and 7 m/s, that coincides with the situation on June 18-24 and 25, respectively. This computational result that the instability is not developed at the wind speed of under 7 m/s agrees well with the realistic situation from June 18 to 25, because the diffusion process is not promoted.

The series of computation from Case 10 to 12 is carried out to see the process of developing the Kelvin-Helmholtz instability. The process of development of the instability and the mixing between upper layer and lower layer can be captured in this series. The two layer is still separated in the case with initial velocity in Fig.4(d). The mixing, however, is induced in contrast with Fig.4(a) to (c). The instability becomes stronger and stronger while the initial velocity increases. When the initial velocity is 7 m/s, the two layer is completely mixed as shown in Fig.4(f).

Fig.5 shows the temperature field in the same cases as Fig.4 with the range of 0 to 1. As the thermal diffusion coefficient is larger than the salinity diffusion coefficient, the boundary layer between the upper layer and the lower layer is thicker than the salinity boundary layer. Thus the instability is difficult to observe in the temperature field, but occurrence of the mixing between the two layers can be seen clearly in Fig.5(f) It is proven that the initial strong impact on the surface can induce the Kelvin-Helmholtz instability that causes the vertical mixing.

Table 2: relationship the wind speed and the correspondent initial velocity according to equation (17))

wind speed [m/s]	correspondent U_{ini} [m/s]
10	0.35
14	0.49
40	1.4

4.4 impact of temperature and salinity differences

Cases 13 to 15 are investigated in order to see the impact of the temperature difference between the two layers. In Case 13, the actual layer thickness in computational domain is taken into account. In Case 14, the situation is expected when the temperature at the upper layer is higher than the lower layer. In Case 15, the situation is expected when the temperature at the sea surface falls below 8°C(Marsaleix, 1998 referred). However, the result for Case 13 is the almost the same as Case

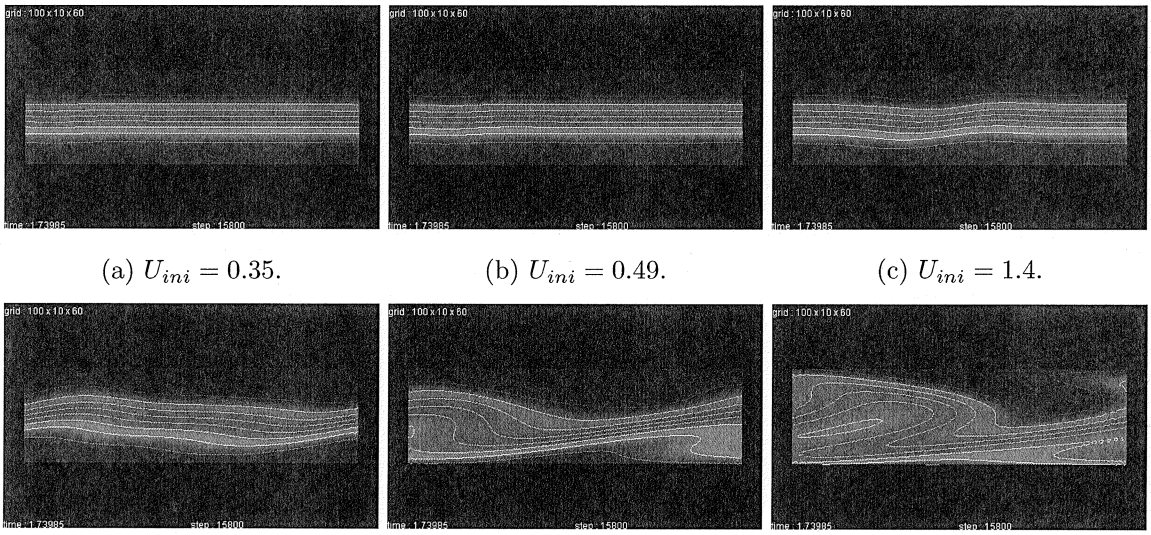

(a) $U_{ini} = 0.35$. (b) $U_{ini} = 0.49$. (c) $U_{ini} = 1.4$.

(d) $U_{ini} = 3$. (e) $U_{ini} = 5$. (f) $U_{ini} = 7$.

Fig.5: Computational results for impact of initial velocity with wind speed of 5 m/s. The shading and contour line represent temperature field. The same range of temperature is used for each case.

8, and results for both Case 14 and 15 are almost the same as Case 10 with respect to the impact on the boundary between the two layers.

Likewise, Case 16 is investigated in order to see the impact of the salinity difference. The actual layer thickness in computational domain is taken into account as well as Case 13. However, the result is almost the same as Case 8 and Case 13. Thus the figures for Cases 13 to 16 are not shown in this paper.

According to these results, the differences of temperature and salinity do not affect the density field as much as the initial velocity and the wind speed condition. The reason is that the thermal and salinity diffusion coefficients and coefficient of volume expansion is so small that the temperature and salinity cannot affect the velocity field.

The parameters used in this computation reflects the physical value, thus it is considered that the temperature and salinity differences do not play an important role for the vertical mixing.

If the temperature can affect the vertical mixing, the temperature of wind may have to be considered. One of the characteristic winds in this region, northern and northwestern wind, is known as cold wind(Millot, 1990). If the air is cold, the wind pressure is bigger than the warm air. This suggests that the vertical mixing is promoted in winter and the stratification is favorable in summer.(Millot, 1990)

5 Conclusion

The numerical simulation for Kelvin-Helmholtz instability is carried out. The following results are found out:

1) the initial velocity gives more impact on the instability at the boundary than the wind force or temperature differences,

2) the initial strong impact on the surface can induce the Kelvin-Helmholtz instability that causes the vertical mixing.

References

[1] Estournel, C. 2001 The Rhone river plume in unsteady conditions: numerical and experimental results. Estuarine, Coastal and Shelf Science **53**, 25-38

[2] Estournel, C., Marsaleix, P., Auclair, F., Julliand, C., Vehil, R., 2003 Observations and modelisation of the winter coastal oceanic circulation in the Gulf of Lions under wind conditions influenced by the continental orography

(FETCH experiment). J. Geophys. Res. **108** (C3), 8059

[3] Kashiwamura, M., Yoshida, S. 1978 Outflow dynamics at a river mouth. Proceedings of the 16th Coastal Engineering Conference, ASCE Hamburg, pp. 2925-2944.

[4] Komurasaki, S. 2007 Numerical simulation of salt finger type convection. RIMS Kokyuroku **1539**, 70-78

[5] Madsen, O. S. 1977 A realistic model of the wind-induced Ekman boundary layer, Journal of Physical Oceanography **7**, pp. 248-255

[6] Marsaleix, P., Estournel, C., Kondrachoff, V., Vehil, R. 1998 A numerical study of the formation of the Rhone river plume. J. Mar. Syst. **14**, 99-115

[7] Millot, C. 1990 The Gulf of Lions' hydrodynamics. Continental Shelf Research **10** (9-11), 885-894

Akiko Mano
Department of Computer Science, Ochanomizu University, Ohtsuka, Bunkyo-ku, Tokyo 112-8610, Japan
g0870609@edu.cc.ocha.ac.jp

Tetuya Kawamura
Department of Computer Science, Ochanomizu University, Ohtsuka, Bunkyo-ku, Tokyo 112-8610, Japan
kawamura@is.ocha.ac.jp